Suboptimal control for drag reduction via suppression of near-wall Reynolds shear stress

Koji Fukagata *, Nobuhide Kasagi

Department of Mechanical Engineering, The University of Tokyo, Hong 7-3-1, Bunkyo-ku, Tokyo 113-8656, Japan

Abstract

We propose a new suboptimal control law for drag reduction in wall-turbulence, which requires the streamwise wall-shear signal only. The cost function is designed to reduce the near-wall Reynolds shear stress that is directly related to the turbulent skin friction drag. The suboptimal solution to minimize the cost function is analytically derived by using the procedure proposed by Lee et al. [J. Fluid Mech. 358 (1998) 245]. Direct numerical simulation of turbulent pipe flow shows that the friction drag can be successfully reduced by the derived control law. Moreover, the sign of Reynolds shear stress in the near-wall layer is found to be reversed with the present control.
© 2004 Elsevier Inc. All rights reserved.

Keywords: Turbulence; Control; Control theory; Drag reduction; Direct numerical simulation; Reynolds shear stress

1. Introduction

For successful development of an active feedback control system for drag reduction in wall-bounded turbulent flow, the effectiveness of the control scheme used as well as the performance of the hardware components such as sensors and actuators is of great importance.

Control schemes may be classified into two types, i.e., explicit and implicit schemes. The explicit scheme is one in which the control input of the actuator i, ϕ_i, is explicitly given by a function of sensor signals. On the other hand, the implicit scheme, such as the optimal control (e.g., Bewley et al., 2001) only describes a relation to be satisfied (i.e., a cost function to be minimized) and requires iterative procedures to determine the control input. While such implicit schemes are useful to explore the possibility of drag reduction control, the explicit schemes are suitable for implementation in the real applications, where real-time computation of the actuation signal is required.

In the last decade, various explicit control laws were developed and assessed by using direct numerical simulation (DNS) of controlled turbulent flow. Choi et al.

(1994) proposed the so-called opposition control, in which blowing/suction velocity is given at the wall so as to oppose the velocity components at a virtual detection plane located above the wall. They attained about 25% drag reduction by this extremely simple control law in their DNS of turbulent channel flow at low Reynolds numbers. Subsequently, several attempts were made to develop control laws using the information measurable at the wall. Lee et al. (1997) used a neural network and found a control law in which the control input is given as a weighted sum of the spanwise wall-shear stresses, $(\partial w/\partial y)_w$, measured around the actuator. Series of analytical solutions of the control input to minimize the cost function was derived by Lee et al. (1998) in the framework of the suboptimal control. Their DNS of channel flow at $Re_\tau \simeq 110$ showed 16–22% drag reduction when $(\partial w/\partial y)_w$ (in this case, the control law is quite similar to that obtained by using the neural network mentioned above) or the wall pressure, p_w, was used as the sensor signal.

From a practical point of view, it is desirable to use the streamwise wall-shear stress, $(\partial u/\partial y)_w$, or p_w (or both) as a sensor signal because a streamwise wall-shear stress sensor (Yoshino et al., 2003) and a wall pressure sensor (Löfdahl et al., 1996) of sufficiently small size and high frequency response are becoming available. For the use of p_w, in addition to the work by Lee et al. (1998),

* Corresponding author. Tel.: +81-3-5841-6419; fax: +81-3-5800-6999.

E-mail address: fukagata@thtlab.t.u-tokyo.ac.jp (K. Fukagata).

Koumoutsakos (1999) presented a scheme to control the vorticity flux, and succeeded to reduce the friction drag in his DNS.

For the use of $(\partial u / \partial y)_w$, however, development of an effective control law seems more difficult. Lee et al. (1998), who developed the above-mentioned $(\partial w / \partial y)_w$- and p_w-based schemes, also presented a suboptimal solution based on $(\partial u / \partial y)_w$. The cost functional was given by

$$\mathscr{I}(\phi) = \frac{\ell}{2A\,\Delta t} \int_S \int_t^{t+\Delta t} \phi^2 \, \mathrm{d}t \, \mathrm{d}S$$
$$+ \frac{1}{2A\,\Delta t} \int_S \int_t^{t+\Delta t} \left(\frac{\partial u}{\partial y} \Big|_w \right)^\alpha \mathrm{d}t \, \mathrm{d}S. \tag{1}$$

Here, ϕ denotes the control input, i.e., the blowing/suction velocity at the wall, A is the area of wall, Δt is the time-span for optimization, and ℓ is the price of control. The power to the wall shear, α, was chosen as 1 or 2. The use of $\alpha = 1$ led to a trivial solution, i.e., $\phi = 0$. With $\alpha = 2$, the derived control law was expressed in the Fourier space as

$$\hat{\phi} = -\frac{\mathrm{i}k_x}{k} \frac{\widehat{\partial u}}{\partial y} \Big|_w, \tag{2}$$

where the hat denotes the Fourier component, k_x is the streamwise wavenumber, $k = \sqrt{k_x^2 + k_z^2}$ is the two-dimensional absolute wavenumber in the streamwise–spanwise plane, and $\mathrm{i} = \sqrt{-1}$. Unfortunately, however, the friction drag was not reduced.

When the dynamics of the system is described by linearized equations, as is in this case, modification of any state variable Δu due to the control input ϕ can symbolically be expressed as

$$\Delta \hat{u}_{mn} = f_{mn}(\hat{\phi}_{mn}), \tag{3}$$

where m and n are the mode numbers and f denotes a mapping function. This indicates, a matter of course, that the interaction occurs only within the same wavenumber. Based on this fact, the following analysis can be made on the cost functional of Eq. (1).

(1) For $\alpha = 1$, the second term of the cost function consists of $(m, n) = (0, 0)$ mode only. Modification of this term is not possible under the zero net-flux constraint usually imposed, i.e., $\hat{\phi}_{00} = 0$.
(2) For $\alpha = 2$, the cost function is decomposed as

$$\mathscr{I}(\phi) = \frac{\ell}{2A} \int_t^{t+\Delta t} \int_S \phi^2 \, \mathrm{d}S + \frac{1}{2A} \int_t^{t+\Delta t} \int_S \left(\frac{\partial u'}{\partial y} \Big|_w \right)^2 \mathrm{d}S$$
$$+ \frac{1}{2} \int_t^{t+\Delta t} \left(\frac{\partial U}{\partial y} \Big|_w \right)^2, \tag{4}$$

where U denotes the mean velocity. Modification of the third term (i.e., the mean wall-shear) is not possible due to the same reason as that for the case of

$\alpha = 1$. The second term, i.e., the fluctuation component, is manipulable.

As analyzed above, the non-trivial solution for the streamwise shear-based suboptimal control, i.e., Eq. (2), actually targets at suppression of the fluctuating component of the streamwise wall-shear, but not the mean component. Although reduction of the friction drag may be attainable by choosing such a target, as is demonstrated by Lee et al. (2001) who uses a two-dimensional linear-quadratic-Gaussian (LQG)/loop-transfer recovery (LTR) controller, the resulting drag reduction effect is merely a byproduct (Lee et al., 2001).

In the present study, we choose a manipulable (i.e., fluctuating) quantity which is more directly related to the skin friction drag, i.e., the near-wall Reynolds shear stress, as the target of suppression. By using intuitive and suboptimal approaches, we attempt to develop a simple algebraic control law which requires $(\partial u / \partial y)_w$ only as the sensor information.

2. Control strategy

An incompressible flow is considered throughout the present study. Under the condition of constant flow rate, the skin friction coefficient in fully developed channel and pipe flows, defined by $C_f = \overline{\tau_w^*} / [(1/2)\rho^* U_b^{*2}]$, can be decomposed as

$$C_f = \frac{12}{Re_b} + 12 \int_0^1 2(1-y)(-\overline{u'v'}) \, \mathrm{d}y \tag{5}$$

and

$$C_f = \frac{16}{Re_b} + 16 \int_0^1 2r \overline{u_r' u_z'} r \, \mathrm{d}r, \tag{6}$$

respectively (Fukagata et al., 2002). The coordinate system is shown in Fig. 1. Here, all variables without superscript are those non-dimensionalized by the channel half-width, δ^*, or the pipe radius, R^*, and twice the bulk mean velocity, $2U_b^*$, whereas dimensional variables
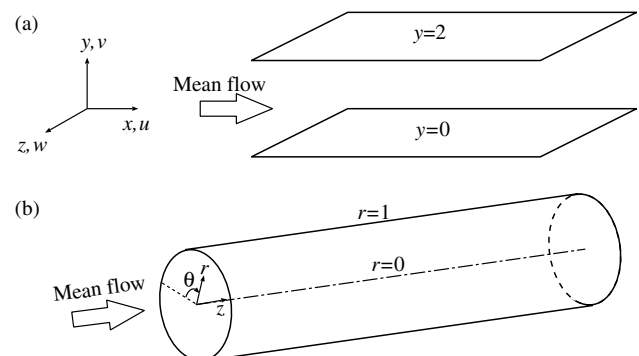

Fig. 1. Coordinate system: (a) channel; and (b) pipe.

are denoted by the superscript $*$. The bulk Reynolds number is defined as

$$Re_b = \frac{2U_b^* \delta^*}{v^*} \quad \text{or} \quad Re_b = \frac{2U_b^* R^*}{v^*}. \tag{7}$$

The overbar ($\bar{\cdot}$) and prime ($\cdot'$) denote the mean and fluctuation components of the Reynolds decomposition. Eqs. (5) and (6) indicate that the skin friction coefficient is decomposed into two parts. One is the laminar contribution given by the well-known laminar solution, and the other is the turbulent contribution, which is proportional to the weighted integral of Reynolds shear stress.

Fig. 2 shows the weighted Reynolds stress appearing in Eq. (6) (i.e., $2r^2\overline{u_r'u_z'}$), in a pipe flow controlled by the opposition control law with different detection plane heights, y_d^{+u}. The difference in the areas covered by the controlled and uncontrolled flow curves is directly proportional to the drag reduction by control. The maximum drag reduction rate is obtained with $y_d^{+u} = 15$. It is clear that most of the drag reduction is attributed to the suppression of Reynolds stress in the near-wall layer. As reported in the study of opposition control (Choi et al., 1994; Hammond et al., 1998; Fukagata and Kasagi, 2003), the drag reduction rate decreases when too high detection plane is used. The case of $y_d^{+u} = 23$ shown in Fig. 2 corresponds the case in which the drag recover to that of the uncontrolled flow. The Reynolds stress at the half-height of the detection plane ($y^{+u} = 12$), around where a formation of virtual wall (Hammond et al., 1998) is expected, is still much lower than that of the uncontrolled flow. The recovery of drag resulted by the use of higher detection plane is rather due to the drastic increase of the Reynolds stress very near the wall.

Another observation in Fig. 2 is that the Reynolds stress far from the wall is also suppressed, although the amount of suppression is relatively small. This can be explained as an indirect effect due to a propagation of the change of Re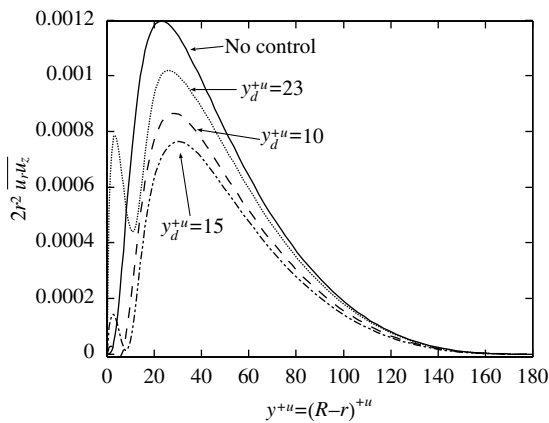ynolds stress in the near-wall layer. In our recent study (Fukagata and Kasagi, 2003), where the opposition control is applied partially to wall, the Reynolds stress profile near the wall drastically changes due to the direct suppression at the beginning of controlled region and the distribution far from the wall changes gradually following the quick change in the near-wall region. Although the control input in that example is switched on in space, a similar phenomenon is expected when the control is turn on at a certain time to a fully developed uncontrolled flow.

The information above suggests that suppression of the near-wall Reynolds shear stress is of primary importance in order to reduce the skin friction drag. Once the near-wall Reynolds shear stress is suppressed, its propagation toward the outer layer is also expected to result in an additional amount of drag reduction. Note that the importance of Reynolds shear stress for drag reduction is pointed out also by Bewley and Aamo (2004), who independently derive an integral relation essentially similar to Eq. (5).

3. Intuitive control

As is well known, the positive Reynolds shear stress (i.e., $-\overline{u'v'} > 0$) near the wall is a consequence of the dominance of the sweep/ejection motions, as is schematically drawn in Fig. 3a. Therefore, an intuitive control strategy in order to attenuate the Reynolds stress in the vicinity of the wall is to give the blowing/suction velocity at the wall proportional to the local wall-shear fluctuation, so that blowing is applied to the high-speed region and suction to the low-speed region (see, Fig. 3b). Thus, with the intuitive control law, the control input ($\phi(x,z,t) = v(x,0,z,t)$ for a channel and $\phi(\theta,z,t) = u_r(1,\theta,z,t)$ for a pipe) can be expressed as

$$\phi = \alpha \left.\frac{\partial u'}{\partial y}\right|_w \quad \text{or} \quad \phi = \alpha \left.\frac{\partial u_z'}{\partial r}\right|_w \tag{8}$$

for a channel or a pipe, respectively. Here, α is the amplitude coefficient that, if dimensional, has a dimension of length.

Fig. 2. Weighted Reynolds stress distribution of the opposition-controlled flow with different detection plane heights y_d.
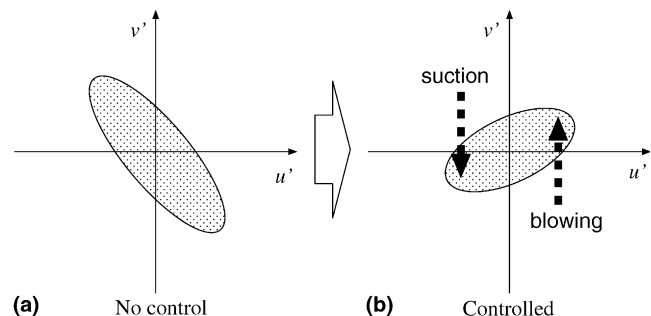

Fig. 3. Schematic of the intuitive control scheme.

4. Suboptimal control

4.1. Cost functional

In the intuitive control introduced above, the actuation signal is determined using only the sensor signal at the identical location. Namely, the modification of flow due to the control input by the neighboring actuators is not accounted for. Such effects are properly taken into account by the suboptimal control procedure described below.

First, we propose a cost functional $\mathscr{J}$ to be minimized as

$$\mathscr{J}_c(\phi) = \frac{\ell}{2A\,\Delta t} \int_S \int_t^{t+\Delta t} \phi^2 \,\mathrm{d}t\,\mathrm{d}S$$
$$+ \frac{1}{2A\,\Delta t} \int_S \int_t^{t+\Delta t} (-u'v')_{y=Y}\,\mathrm{d}t\,\mathrm{d}S \qquad (9)$$

for a channel flow and

$$\mathscr{J}_p(\phi) = \frac{\ell}{A\,\Delta t} \int_S \int_t^{t+\Delta t} \phi^2 \,\mathrm{d}t\,\mathrm{d}S$$
$$+ \frac{1}{A\,\Delta t} \int_S \int_t^{t+\Delta t} (u'_r u'_z)_{r=(R-Y)}\,\mathrm{d}t\,\mathrm{d}S \qquad (10)$$

for a pipe flow, respectively. Here, ϕ denotes the control input, i.e., the blowing/suction velocity at the wall, A is the area of wall, Δt is the time-span for optimization, and ℓ is the price for the control.

The proposition is to minimize this cost functional under the linearized Navier–Stokes equation. Since a very short time, Δt, is considered here, the linearization is done, similarly to Lee et al. (1998), by temporally discretizing the Navier–Stokes equation so that the advection term does not affect the determination of control input. Namely, by using an explicit scheme for the nonlinear terms and Crank–Nicolson scheme for the linear terms for temporal discritization, the short time dynamics of the system is approximated by the following set of equations:

$$\nabla \cdot \mathbf{u}^{n+1} = 0, \qquad (11)$$

$$\mathbf{u}^{n+1} = \Delta t \left[-\nabla p^{n+1} + \frac{2}{Re_b} \nabla^2 \mathbf{u}^{n+1} \right] + \mathbf{F}^n, \qquad (12)$$

where the superscripts of n and $n+1$ denote the discrete time instances, and $\mathbf{F}$ is the part explicitly integrated, i.e.,

$$\mathbf{F}^n = \mathbf{u}^n + \Delta t \left[-\nabla \cdot (\mathbf{u}^n \mathbf{u}^n) + \frac{2}{Re_b} \nabla^2 \mathbf{u}^n \right]. \qquad (13)$$

The velocity boundary condition on the wall is

$$\mathbf{u}|_w^{n+1} = \phi \mathbf{n}_w, \qquad (14)$$

where $\mathbf{n}_w$ is the wall-normal unit vector.

4.2. Control law for channel flow

As mentioned in Section 1, our purpose is to develop a control law which uses the streamwise wall-shear as the sensor information. Therefore, the Reynolds shear stress above the wall ($y = Y$) appearing in the cost function needs to be evaluated by using the information on the wall. The Taylor-series expansions of the streamwise and wall-normal velocities read

$$u'(Y) = Y \frac{\partial u'}{\partial y}\bigg|_w + \frac{Y^2}{2} \frac{\partial^2 u'}{\partial y^2}\bigg|_w + \mathcal{O}(Y^3) \qquad (15)$$

and

$$v'(Y) = \phi + \frac{Y^2}{2} \frac{\partial^2 v'}{\partial y^2}\bigg|_w + \mathcal{O}(Y^3), \qquad (16)$$

respectively. The leading term for $v'(Y)$ in the absence of the control input is on the second order. With control, however, the zeroth-order term appears. By taking the leading order term of the Taylor-series expansion, the Reynolds stress at $y = Y$ under control is approximated as

$$-u'v'(Y) \simeq -Y\phi \frac{\partial u'}{\partial y}\bigg|_w. \qquad (17)$$

Substitution of Eq. (17) into Eq. (9) yields an approximated cost functional, i.e.,

$$\mathscr{J}_c(\phi) = \frac{\ell}{2A\,\Delta t} \int_S \int_t^{t+\Delta t} \phi^2 \,\mathrm{d}t\,\mathrm{d}S$$
$$- \frac{Y}{2A\,\Delta t} \int_S \int_t^{t+\Delta t} \phi \frac{\partial u'}{\partial y}\bigg|_w \mathrm{d}t\,\mathrm{d}S. \qquad (18)$$

The control input, ϕ, that minimize the cost functional, Eq. (18), can be calculated analytically through the procedure proposed by Lee et al. (1998) as follows. First, the Fréchet differentiation is applied to the cost functional, i.e.,

$$\frac{\mathscr{D}\mathscr{J}_c}{\mathscr{D}\phi}\tilde{\phi} = \frac{\ell}{A\,\Delta t} \int_S \int_t^{t+\Delta t} \phi\tilde{\phi} \,\mathrm{d}t\,\mathrm{d}S$$
$$- \frac{Y}{2A\,\Delta t} \int_S \int_t^{t+\Delta t} \left(\frac{\partial u}{\partial y}\bigg|_w \tilde{\phi} + \phi \frac{\partial q}{\partial y}\bigg|_w \right)\mathrm{d}t\,\mathrm{d}S. \qquad (19)$$

Here, the Fréchet differential is defined by

$$\frac{\mathscr{D}f(\phi)}{\mathscr{D}\phi}\tilde{\phi} = \lim_{\varepsilon\to 0} \frac{f(\phi + \varepsilon\tilde{\phi}) - f(\phi)}{\varepsilon} \qquad (20)$$

and q is the differential state of the streamwise velocity, i.e.,

$$q = \frac{\mathscr{D}u}{\mathscr{D}\phi}\tilde{\phi}. \qquad (21)$$

Next, we consider a two-dimensional Fourier transform defined by

$$f = \sum_m \sum_n \hat{f} \exp(ik_x x + ik_z z), \tag{22}$$

where f represents any variable and the hat denotes its Fourier coefficient. The streamwise and spanwise wavenumbers are defined by $k_x = 2\pi m/L_x$ and $k_z = 2\pi n/L_z$, respectively, $i = \sqrt{-1}$. This two-dimensional discrete Fourier transform is applied to the approximated cost functional, Eq. (18), to yield

$$\frac{\widehat{\mathscr{DI}_c}}{\mathscr{D}\phi}\hat{\tilde{\phi}}^\star = \ell\hat{\phi}\hat{\tilde{\phi}}^\star - \frac{Y}{2}\left(\left.\widehat{\frac{\partial u}{\partial y}}\right|_w \hat{\tilde{\phi}}^\star + \hat{\phi}\left.\widehat{\frac{\partial q}{\partial y}}^\star\right|_w\right), \tag{23}$$

where the superscript $\star$ denotes a complex conjugate and the indices for mode numbers (mn) are omitted for notational simplicity. The modification of the streamwise velocity due to the perturbation field, $\hat{q}$, that appears in Eq. (23) can be determined by solving the Fréchet differential of the state equation (i.e., the linearized Navier–Stokes equation). Since here we consider the same state equation and boundary condition as those used by Lee et al. (1998), i.e., Eqs. (11)–(14), we simply borrow their solution of $\hat{q}$ that reads

$$\hat{q}(y) = \frac{ik_x}{k}\tilde{\phi}\left[\exp(-\sqrt{k^2 + \gamma^2}y) - \exp(-ky)\right], \tag{24}$$

where $k = \sqrt{k_x^2 + k_z^2}$ and the parameter γ is defined by

$$\gamma = \sqrt{\frac{2Re_b}{\Delta t}}. \tag{25}$$

From this solution, the complex conjugate of the wall-shear modification due to the perturbation field can be calculated as

$$\left.\widehat{\frac{\partial q}{\partial y}}^\star\right|_w \simeq \gamma\frac{ik_x}{k}\hat{\tilde{\phi}}^\star, \tag{26}$$

where the same assumption as that used by Lee et al. (1998), i.e., $k^2 \ll \gamma^2$ is used.

Finally, by substituting, Eq. (26) into Eq. (23), we can find the suboptimal control input that makes $(\mathscr{DI}_c/\mathscr{D}\phi)\tilde{\phi} = 0$ for any $\tilde{\phi}$, which can be expressed as

$$\hat{\phi} = \alpha\left[\left.\widehat{\frac{\partial u}{\partial y}}\right|_w + \gamma\frac{ik_x}{k}\hat{\phi}\right] \tag{27}$$

or, by isolating $\hat{\phi}$,

$$\hat{\phi} = \frac{\alpha}{1 - i\alpha\gamma k_x/k}\left.\widehat{\frac{\partial u}{\partial y}}\right|_w. \tag{28}$$

Here, the amplitude coefficient α (cf. Eq. (8)) is related to the predefined parameters, ℓ and Y, by

$$\alpha = \frac{Y}{2\ell}. \tag{29}$$

The first expression, Eq. (27), suggests that this suboptimal control law is essentially similar to the intuitive control, but with the correction term for the modifica-

tion of the flow field due to the control itself. It is worth mentioning that $1/\gamma$ can be interpreted as the influential thickness in time Δt (both non-dimensionalized by δ^* and $2U_b^*$) analogous to that in the Rayleigh's problem. Therefore the product $\alpha\gamma$ appearing in the second expression, Eq. (28) can be interpreted a ratio of control amplitude to its influential thickness. (In dimensional space, too, $\alpha^* = Y^*/\ell$ and $\gamma^* = \sqrt{2/(v^*\Delta t^*)}$ makes the product $\alpha^*\gamma^*$ a dimensionless number.) The difference from the intuitive control becomes larger when the control is strong, i.e., large α, or when the momentum introduced by control during Δt is diffused within a thin layer, i.e., large γ.

In the first step of the present derivation, the Reynolds shear stress above the wall is approximated by using only the leading order term, see, Eq. (17). One may be tempted to include also higher order terms for a better approximation. In that case, however, the control law derived in a similar manner requires other information such as p_w and $(\partial w/\partial y)_w$, too.

4.3. Weights in the physical space

The derived control algorithms can be transformed to the physical space through the inverse discrete Fourier transform, i.e.,

$$\hat{\phi} = \widehat{W}^\star\left.\widehat{\frac{\partial u}{\partial y}}\right|_w \Rightarrow \phi_{k\ell} = \sum_i \sum_j W_{ij}\left.\frac{\partial u}{\partial y}\right|_{w,k+i,\ell+j}, \tag{30}$$

where $\widehat{W}^\star$ is the function preceding $\widehat{(\partial u/\partial y)}_w$ in Eq. (28). The subscripts to the variable in the physical space, i, j, k and ℓ, denote the discrete positions of a sensor or an actuator, e.g., $W_{ij} = W(i\Delta x, j\Delta z)$. Eq. (30) indicates that the control input of an actuator is given by a weighted sum of the streamwise wall-shear around it. Fig. 4 shows the distribution of the weight, W_{ij}, normalized by W_{00} in the case of $\alpha\gamma = 73$. The weight distribution has different characteristics in the streamwise
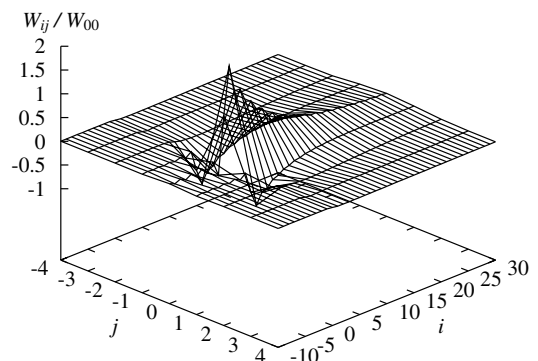

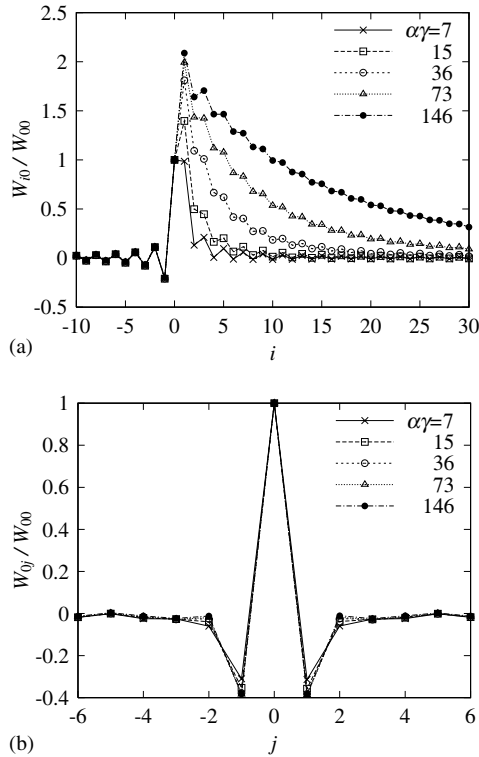Fig. 4. Normalized weights in the physical space ($\alpha\gamma = 73$).

Fig. 5. Dependency of the distribution of weight on the parameter $\alpha\gamma$: (a) streamwise distribution at $j = 0$; and (b) spanwise distribution at $i = 0$.

and spanwise directions. It is symmetric in the spanwise direction and whereas asymmetric in the streamwise direction.

One-dimensional weight distributions on the orthogonal axes, i.e., $j = 0$ and $i = 0$, are depicted in Fig. 5 for different values of $\alpha\gamma$. The streamwise distributions are similar to curves of exponential decrease. The maximum weight appears at the position right downstream of the actuator and its value is dependent on $\alpha\gamma$. The number of downstream sensors that should be accounted for is determined by the parameter, $\alpha\gamma$. On the other hand, the spanwise distribution is nearly independent of the parameter $\alpha\gamma$ and it is similar to a negative second derivative.

Note, if the weighting function in the Fourier space were

$$\widehat{W}^\star = \frac{\alpha}{1 - \mathrm{i}\alpha\gamma k_x} \tag{31}$$

(i.e., omitting the division by k), then the normalized weight in the physical space would be

$$\frac{W(x)}{W(0)} = \begin{cases} 0 & (x < 0), \\ \exp[-x/\alpha\gamma] & (x \geqslant 0). \end{cases} \tag{32}$$

This relation may qualitatively explain the exponential-like decrease of the weight in the streamwise direction.

4.4. Control law for pipe flow

The control law for a pipe flow can be developed similarly by using the Taylor-series expansion of the near-wall Reynolds shear stress, i.e.,

$$u_r' u_z' (1 - Y) = -Y\phi \frac{\partial u_z'}{\partial r}\bigg|_w + \mathcal{O}(Y^2) \tag{33}$$

and the solution of q for pipe flow (Xu et al., 2002), i.e.,

$$\hat{q} = \mathrm{i}\widehat{\rho_w} \frac{k_z \Delta t}{2} \left[\frac{I_m(\gamma r)}{I_m(\gamma)} - \frac{I_m(k_z r)}{I_m(k_z)} \right], \tag{34}$$

where

$$\widehat{\rho_w} = -\frac{2}{\Delta t} \left[\frac{I_m(\gamma)}{I_{m+1}(\gamma)} + \frac{I_m(\gamma)}{I_{m-1}(\gamma)} \right] \hat{\tilde{\phi}} \bigg/ k_p \tag{35}$$

and

$$k_p = k_z \left[\frac{I_{m+1}(k_z)}{I_m(k_z)} \frac{I_m(\gamma)}{I_{m+1}(\gamma)} + \frac{I_{m-1}(k_z)}{I_m(k_z)} \frac{I_m(\gamma)}{I_{m-1}(\gamma)} - 2\frac{k_z}{\gamma} \right]. \tag{36}$$

Here, m is the azimuthal mode number and $I_m(r)$ denotes the mth order modified Bessel function, i.e., $I_m(r) = (-\mathrm{i})^m J_m(\mathrm{i}r)$. The length is non-dimensionalized by R^*, and hence $k_\theta = (2\pi m)/(2\pi R) = m$ and $k = \sqrt{k_z^2 + m^2}$. By this non-dimensionalization and by using the similar assumption as that made for channel, i.e., $k_z^2, m^2 \ll \gamma^2$, the expression above is simplified as compared to the original version of Xu et al. (2002).

Following the similar procedure as that for the channel flow, we obtain the control input, which reads

$$\hat{\phi} = \frac{\alpha}{1 - \mathrm{i}\alpha\gamma\kappa(m, k_z)} \frac{\widehat{\partial u_z}}{\partial r}\bigg|_w. \tag{37}$$

The difference from the solution for channel flow is absorbed into the factor, $\kappa(m, k_z)$. As can be imagined from Eqs. (34)–(36), the exact expression of $\kappa(m, k_z)$ is highly complicated. However, under the condition of $|m| \ll \gamma$, the asymptotic expression for the modified Bessel function, i.e.,

$$I_m(\gamma) \simeq \frac{1}{\sqrt{2\pi\gamma}} \exp(\gamma) \tag{38}$$

simplifies the expression of $\kappa(m, k_z)$, as

$$\kappa(m, k_z) = \left[\left(\frac{1}{2\gamma} + 1 \right) \frac{I_m(k_z)}{I_m'(k_z)} - \frac{1}{\gamma} \right], \tag{39}$$

where $I_m'(r)$ is the radial derivative of $I_m(r)$. The parameter γ is usually much larger than unity. In that case, Eq. (39) can be further simplified to result in

$$\kappa(m, k_z) = \frac{I_m(k_z)}{I_m'(k_z)}. \tag{40}$$

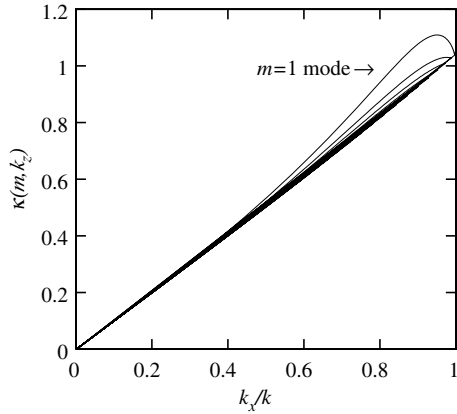The correlation between the wavenumber-dependent parts, i.e., k_x/k for channel and $\kappa(m, k_z)$ for pipe, is

Fig. 6. Correlation between k_x/k for channel and $\kappa(m,k_z)$ for pipe.

Fig. 7. Drag reduction rate, R_D (with the coarser grid, except for a finer grid computation with $\alpha\gamma = 36$ denoted by '●').

shown in Fig. 6. The correlation is nearly linear for higher wavenumbers. As can be imagined from the geometrical difference, the largest deviation is observed at the lowest azimuthal wavenumber ($m = 1$).

The distribution of the weight in the physical space is found to be nearly the same as that for the channel flow.

5. Performance test

Performance of the proposed control laws is assessed by DNS of turbulent pipe flow. First, about 40 runs are performed for the present suboptimal control with different values of the parameters α and γ.

The DNS code is based on the energy conservative finite difference method for the cylindrical coordinate system (Fukagata and Kasagi, 2002). The time integration is done by using the low storage third-order Runge–Kutta/Crank–Nicolson scheme (see, e.g., Spalart et al., 1991). The bulk mean velocity U_b is kept constant, and the Reynolds number is $Re_b = 5300$ ($Re_\tau \simeq 180$ for uncontrolled flow). The computational domain has a longitudinal length of $L = 20R$ and the periodic boundary conditions are applied at both ends. The specification of the computational grid is summarized in Table 1. The coarser grid system is used for the parameter study, while the finer grid system is for accumulation of detailed statistics. It has been verified in the DNS of opposition controlled flows that even the coarser grid system used here is sufficient to evaluate the drag reduction rate (Fukagata and Kasagi, 2003).
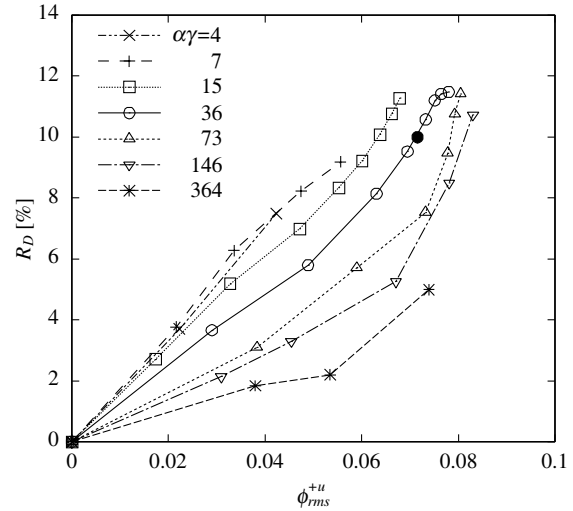
Fig. 7 shows the time-averaged drag reduction rate, R_D, as a function of the resulting amplitude of control input, ϕ_{rms}^{+u}, for different values of $\alpha\gamma$. Here, the superscript of $+u$ denotes the wall unit of the uncontrolled flow. The drag reduction rate increases with the increase of amplitude. Relatively large drag reduction rate was obtained when $15 \leqslant \alpha\gamma \leqslant 146$ with the values of α that result in $0.065 < \phi_{rms}^{+u} < 0.085$. This amplitude is comparable to that of the opposition control with the detection plane height of $y_d^{+u} \simeq 10$. The efficiency of the control is slightly better with smaller value of $\alpha\gamma$. For instance, amplitude of $\phi_{rms}^{+u} \simeq 0.063$ is required to obtain 10% drag reduction with $\alpha\gamma = 15$, whereas $\phi_{rms}^{+u} \simeq 0.079$ with $\alpha\gamma = 73$. From the definition of α and γ, this deterioration for large value of $\alpha\gamma$ is explained by that the approximation of Reynolds stress above the wall by the Taylor expansion becomes inaccurate for large Y, as well as by that the control becomes cheaper.

In Fig. 7, drag reduction rates only of the successful cases are plotted and the cases in which the drag increased (and often the computation diverged) are excluded. For example, for $\alpha\gamma = 73$ the drag was reduced by 11.5% with $\phi_{rms}^{+u} \simeq 0.08$, but the drag increased at a slightly stronger control due to instability in the near-wall layer. In any cases examined with $\phi_{rms}^{+u} > 0.085$, the drag was not reduced. The instability for large amplitude of control can be explained by the form of the present control law. The first term in the right-hand side

Table 1
Number of grids (N_r, N_θ, N_z) and grid spacing ($\Delta r, R\Delta\theta, \Delta z$)

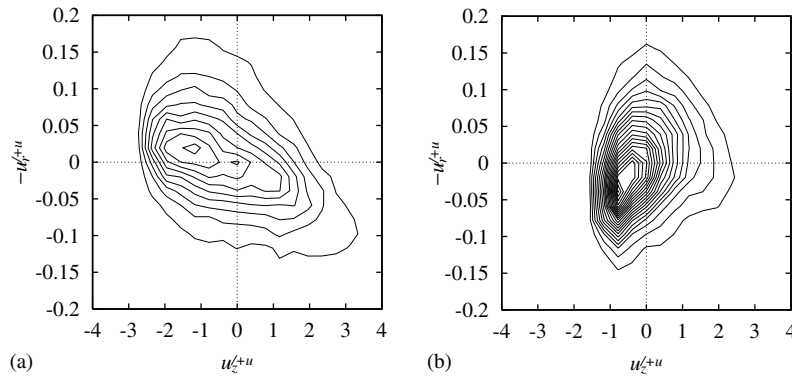|	N_r	N_θ	N_z	Δr^{+u}	$(R\Delta\theta)^{+u}$	Δz^{+u}
Finer grid	96	128	512	0.46–2.99	8.84	7.03
Coarser grid	48	128	256	0.95–6.11	9.03	14.4

Fig. 8. Joint probability density distribution of the streamwise and wall-normal velocity fluctuations at $y^{+u} \simeq 5$: (a) without control; and (b) with the present suboptimal control.

of Eq. (27) is associated with the flow information, but the second term is a function of the control input itself. Therefore, for too large ϕ, the control input is determined by itself regardless of the status of the flow. As the result, the system becomes unstable. The simulations are also performed by dynamically adjusting the amplitude coefficient so that ϕ_{rms} becomes constant in time. In those cases, the control amplitude can be increased up to $\phi_{\mathrm{rms}}^{+u} \simeq 0.17$. The drag reduction rate, however, decreases for $\phi_{\mathrm{rms}}^{+u} > 0.08$ and the maximum drag reduction rate is unchanged from the cases of the constant amplitude coefficient described above.

Fig. 8 shows the joint probability density function (PDF) of the streamwise and wall-normal velocity fluctuations near the wall ($y^{+u} \simeq 5$) of the case computed on the finer grid system, i.e., $\alpha\gamma = 36$ and $\phi_{\mathrm{rms}}^{+u} \simeq 0.07$. The joint PDF exhibits a similar change to what we initially expected (Fig. 3). The sweep and ejection are suppressed, whereas the low-speed inward and high-speed outward motions are enhanced by the present control.

The profile of the Reynolds shear stress of the corresponding case is shown in Fig. 9. Again, the near-wall Reynolds stress is suppressed with the present control as

we initially intended. As can be seen from the comparison, the profile of the present control is nearly the same as that of the opposition control (denoted as v-control) with $y_{\mathrm{d}}^{+u} = 5$. A small difference between them can be noticed in the region of $0 < y^{+u} < 5$, where the sign of the Reynolds shear stress is reversed with the present control. In Fig. 9, comparison is also made with the opposition control with $y_{\mathrm{d}}^{+} = 15$, in which the Reynolds stress around $5 < y^{+u} < 10$ is mostly suppressed to result in a higher drag reduction rate ($\simeq 25\%$). The direct suppression with the present control seems to occur merely in the region of $0 < y^{+u} < 5$. These comparisons suggest a possibility of further drag reduction by modification of control law so that a largely negative Reynolds shear stress is created in the near-wall layer or the Reynolds shear stress farther from the wall is directly suppressed.

Contours of the wall-shear stress fluctuation are depicted in Fig. 10. As is well known, a streaky structure of wall-shear can be observed in the uncontrolled flow. With the present control, the wall-shear fluctuation is drastically reduced and it forms somewhat circular structures. This change is slightly different from the results of most of the previous controls (e.g., Choi et al., 1994; Lee et al., 1998; Endo et al., 2000; Lee et al., 2001) in which elongation of streaky structure was observed. This circular structure becomes more pronounced as the increase of control amplitude, which seems to be related to the above-mentioned instability for excessively large values of ϕ_{rms}.

For the intuitive control scheme, Eq. (8) or $\gamma \to 0$ limit of the present suboptimal control law, the computation is very unstable and drag reduction is not observed with any value of the parameter examined. Such unstable behavior is illustrated in Fig. 11, in which time trace of ϕ of one sample actuator is plotted. For comparison, similar time traces for the present suboptimal control and two suboptimal control schemes by Lee et al. (1998), i.e., the streamwise wall-shear-based control, Eq. (2), and the spanwise wall-
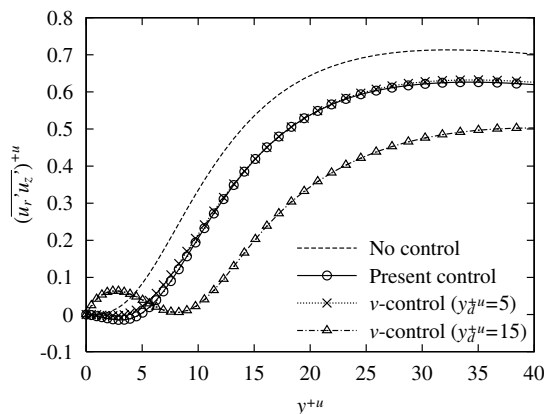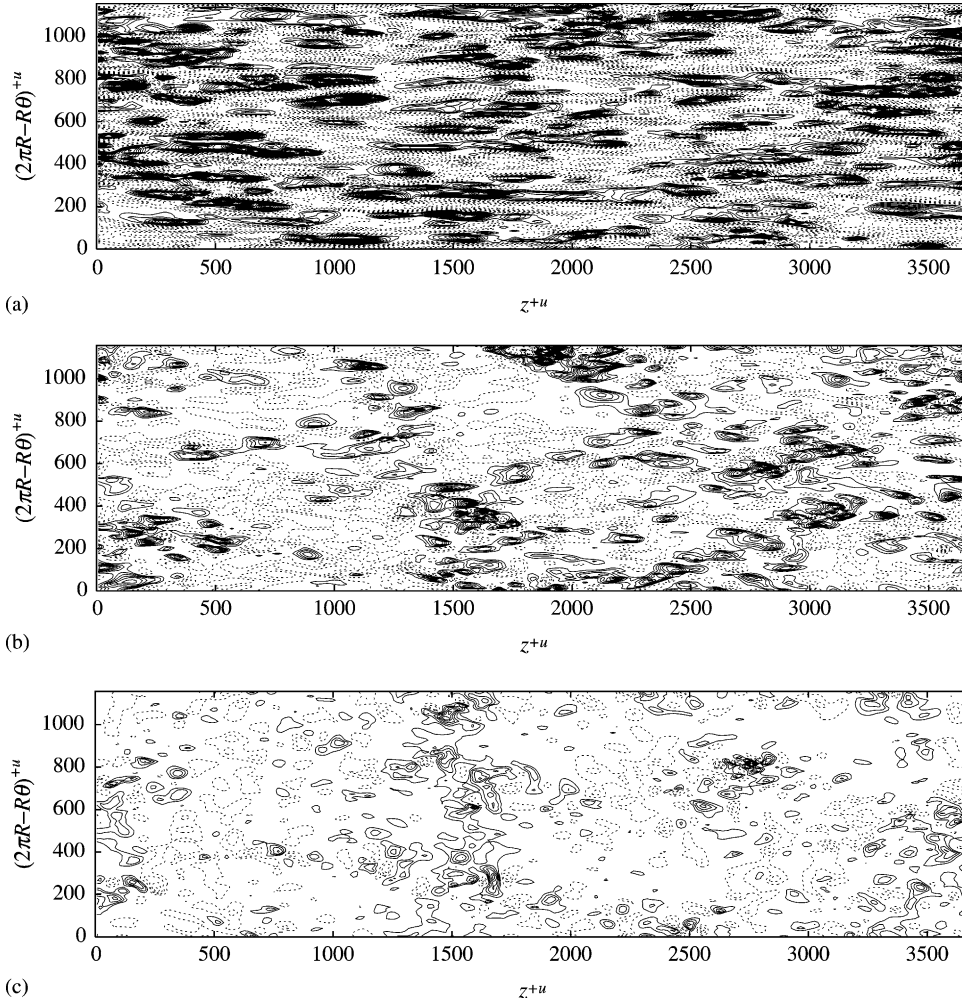

Fig. 9. Reynolds shear stress.

Fig. 10. Contours of streamwise wall-shear stress fluctuation, $-(\partial u'_z/\partial r)_{\mathrm{w}}$: (a) without control; (b) present control ($\alpha\gamma = 36$) with $\phi^{+\mathrm{u}}_{\mathrm{rms}} \simeq 0.063$; and (c) $\phi^{+\mathrm{u}}_{\mathrm{rms}} \simeq 0.078$. Increment is 0.1 wall unit and negative contours are dashed.
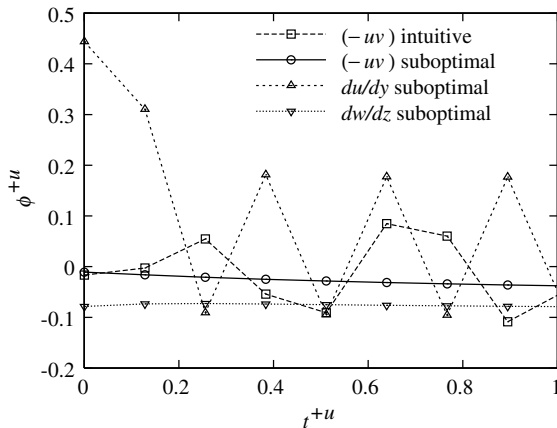

Fig. 11. Time trace of control input of an actuator with different control schemes.

shear-based control, $\hat{\phi} = \mathrm{i}(k_z/k)(\partial \hat{w}/\partial y)_{\mathrm{w}}$, are also shown. In all cases, the magnitude of control input is fixed at $\phi^{+\mathrm{u}}_{\mathrm{rms}} = 0.08$. It is clear that two schemes that

successfully reduce the drag (i.e., the present $(-uv)$-based suboptimal control law and the $(\partial w/\partial y)$-based suboptimal control law give almost constant control input in this short period of time (1 wall unit time), whereas those do not reduce the drag give oscillatory control input. Note that the CFL number in the near-wall region is less than 0.1 so that this instability is not a purely numerical one. The instability is probably due also to the coupling between the dynamics of the plant (i.e., fluid flow) and the controller.

6. Summary and conclusions

Based on the knowledge on the componental contribution to the skin friction (Fukagata et al., 2002), an alternative cost functional for drag reduction, which incorporates the near-wall Reynolds shear stress, was proposed in the framework of the suboptimal control.

The control input to minimize that cost functional was analytically obtained by using the method proposed by Lee et al. (1998). Only the streamwise wall-shear signal, which is the sole quantity usable in the physical experiment at this moment, is required to determine the control input. Different from any other explicit control laws previously proposed, the weighting function has a practically two-dimensional distribution, which is asymmetric in the streamwise direction and symmetric on the spanwise direction.

DNS of pipe flow at $Re_\tau \simeq 180$ with the present control law showed a clear drag reduction effect, which could not be attained by the previous streamwise wall-shear-based suboptimal control law (Lee et al., 1998). As initially intended, the Reynolds shear stress in the near-wall layer can be successfully suppressed. The modification of the profile is basically similar to that by the opposition control with a low detection plane height. In addition, the sign of the Reynolds shear stress is reversed in the region of $0 < y^{+u} < 5$.

Although the drag reduction rate attained by the present algorithm was small, the result suggests that further drag reduction may be possible, if the structure farther from the wall can be directly manipulated such as in the opposition control, or if the Reynolds shear stress in the near-wall layer can be made strongly negative. In order to realize these ideas, one has to overcome the problem of instability, which is revealed to be common to several unsuccessful control laws. The cause for this instability presumably lurks in the coupling between the plant and the controller. The details, however, should be further investigated.

Acknowledgements

References

Bewley, T.R., Aamo, O.M., 2004. A "win–win" mechanism for low-drag transients in controlled 2D channel flow and its implications for sustained drag reduction. J. Fluid Mech. 499, 183–196.

Bewley, T.R., Moin, P., Temam, R., 2001. DNS-based predictive control of turbulence: an optimal benchmark for feedback algorithms. J. Fluid Mech. 447, 179–225.

Choi, H., Moin, P., Kim, J., 1994. Active turbulence control for drag reduction in wall bounded flows. J. Fluid Mech. 262, 75–110.

Endo, T., Kasagi, N., Suzuki, Y., 2000. Feedback control of wall turbulence with wall deformation. Int. J. Heat Fluid Flow 21, 568–575.

Fukagata, K., Kasagi, N., 2002. Highly energy-conservative finite difference method for the cylindrical coordinate system. J. Comput. Phys. 181, 478–498.

Fukagata, K., Kasagi, N., 2003. Drag reduction in turbulent pipe flow with feedback control applied partially to wall. Int. J. Heat Fluid Flow 24, 480–490.

Fukagata, K., Iwamoto, K., Kasagi, N., 2002. Contribution of Reynolds stress distribution to the skin friction in wall-bounded flows. Phys. Fluids 14, L73–L76.

Hammond, E.P., Bewley, T.R., Moin, P., 1998. Observed mechanisms for turbulence attenuation and enhancement in opposition-controlled wall-bounded flows. Phys. Fluids 10, 2421–2423.

Koumoutsakos, P., 1999. Vorticity flux control for a turbulent channel flow. Phys. Fluids 11, 248–250.

Lee, C., Kim, J., Babcock, D., Goodman, R., 1997. Application of neural networks to turbulence control for drag reduction. Phys. Fluids 9, 1740–1747.

Lee, C., Kim, J., Choi, H., 1998. Suboptimal control of turbulent channel flow for drag reduction. J. Fluid Mech. 358, 245–258.

Lee, K.H., Cortelezzi, L., Kim, J., Speyer, J., 2001. Application of reduced-order controller to turbulent flows for drag reduction. Phys. Fluids 13, 1321–1330.

Löfdahl, L., Kälvesten, E., Stemme, G., 1996. Small silicon pressure transducers for space–time correlation measurements in a flat plate boundary layer. J. Fluids Eng. 118, 457–463.

Spalart, P.R., Moser, R.D., Rogers, M.M., 1991. Spectral methods for the Navier–Stokes equations with one infinite and two periodic directions. J. Comput. Phys. 96, 297–324.

Xu, C.-X., Choi, J.-I., Sung, H.J., 2002. Suboptimal control for drag reduction in turbulent pipe flow. Fluid Dyn. Res. 30, 217–231.

Yoshino, T., Suzuki, Y., Kasagi, N., Kamiunten, S., 2003. Optimum design of micro thermal flow sensor and its evaluation in wall shear stress measurement. In: Proc. IEEE Int. Conf. MEMS'03, Kyoto, January 2003, pp. 193–196.